An Active Quasi-Circulator IC with Source-Follower DAC for 1–255 MHz Spectroscopic Impedance Plethysmography

Sharisse Poff[1], Nicholas E. Allen[1], Jacob Anderson[1], Yi-Kai Wu[2], Benjamin Boyack[1], Chuan-Tai Chou[3], Armin Tajalli[4], Karl F. Warnick[1], David V. Anderson[5], Chia-Hung Chen[3], Marcus Julian[6], Robert C. Davis[1], and Shiuh-hua Wood Chiang[1] (wochiang@byu.edu)
[1]*Brigham Young University;* [2]*National Taiwan University;* [3]*National Yang Ming Chiao Tung University;*
[4]*University of Utah;* [5]*Georgia Institute of Technology;* [6]*Tula Health, Inc.*

***Abstract*—Resonance-based impedance measurements of human tissue correlate with blood glucose levels at excitations from tens of MHz to over 100 MHz. Thus, we present an IC that measures spectroscopic impedance plethysmography up to 255 MHz. The circuit incorporates an active quasi-circulator to maximize sensitivity and a source-follower DAC to buffer the excitation signal while presenting a programmable resistance tuned to the tissue impedance. The excitation signal is generated on-chip, and I/Q mixers downconvert the output for digitization. Electrical and human test results demonstrate, for the first time, spectroscopic plethysmography for resonance-based measurements across a wide range of frequencies and various load impedances.**

***Index Terms*—Active quasi-circulator, source-follower DAC, impedance measurement, impedance plethysmography, spectroscopic plethysmography**

I. Introduction

Impedance measurement is a promising avenue for non-invasive glucose monitoring. Specifically, impedance measurements that monitor resonance exhibit good correlation with glucose levels at excitations from tens of MHz to over 100 MHz [1], [2]. Such measurements are desirable at these frequencies as opposed to the kHz range because the effects of electrode polarization decrease as frequency increases [1], [3], [4]. Additionally, impedance measurements that are plethysmographic can detect time-dependent changes caused by blood flow during a heartbeat. Such measurements are needed to separate arterial blood signals, which contain stronger glucose information, from interstitial fluid signals [5]–[9]. Although plethysmography has been measured by various systems, none have operated from tens to over 100 MHz. Moreover, plethysmographic measurements across a range of frequencies—spectroscopic plethysmography—have not previously been demonstrated. We anticipate that such measurements could enable resonance-based monitoring with higher selectivity for arterial glucose than previous work.

We propose an IC that performs spectroscopic impedance plethymography for arterial blood monitoring up to 255 MHz. The core of the IC is an active quasi-circulator (AQC) that measures impedance through the principle of signal nulling by tuning an amplifier with a novel source-follower digital-to-analog converter (SF DAC). This nulling functionality maximizes sensitivity to plethysmographic signals to achieve sub-Ω measurements across a wide range of baseline impedances. On-chip excitation signal generation facilitates resonance-based measurements through real-time tunability from 1–255 MHz. We demonstrate spectroscopic plethysmography across this frequency range on human subjects, thus laying the groundwork to enhance future studies on blood glucose–impedance correlations.

This work was supported by Tula Health, Inc. Chip fabrication was supported by Taiwan Semiconductor Research Institute (TSRI).

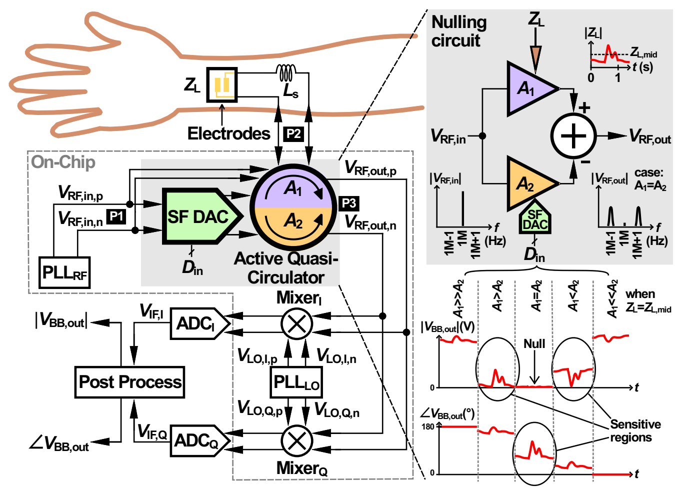

Fig. 1. Proposed spectroscopic impedance plethysmography system. Expanded visual shows how AQC and SF DAC form a nulling circuit. The human tissue (Z_L) affects A_1 and D_{in} affects A_2 to increase sensitivity to changes in Z_L.

II. Architecture

The proposed IC is incorporated into the spectroscopic plethysmography system shown in Fig. 1. A phase-locked loop (PLL_{RF}) sends an excitation signal ($V_{RF,in}$) into port 1 (P1) of the active quasi-circulator (AQC), where it travels through two separate paths with gains of A_1 and A_2. The value of A_1 is determined by the tissue impedance of the human wrist (Z_L) at port 2 (P2). The value of A_2 is controlled

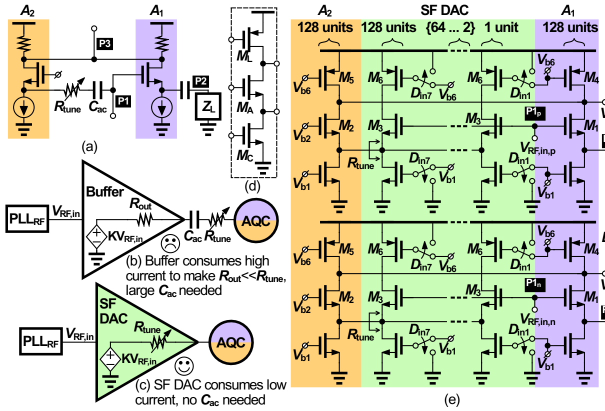

Fig. 2. (a) AQC implementation with R_{tune} as tuning mechanism for nulling function. (b) Problem of high current needed to buffer $V_{RF,in}$ prior to AQC. (c) Proposed SF DAC absorbs R_{tune} into its R_{out} to reduce power by 20×, and eliminates C_{ac}. (d) Unit cell used to form AQC and SF DAC. (e) Details of proposed AQC and SF DAC consisting of binary-weighted unit cells.

by D_{in}, a digital control word that programs the SF DAC's output resistance. At port 3 (P3), the signals from the A1 and A2 paths are combined to produce the output signal: $V_{RF,out} = V_{RF,in}(A_2 - A_1)$. By tuning A_2 to equal or nearly equal A_1 (as described in Section III), a nulling circuit is formed. This nulling functionality cancels the baseline impedance, creates high $\Delta|V_{RF,out}|/\Delta Z_L$ by inducing a slope near the null, and creates high $\Delta\angle V_{RF,out}/\Delta Z_L$ by inducing a 180° phase shift as the null is crossed. For complex Z_L, the capacitive component of Z_L decreases sensitivity by causing the phase difference between A_1 and A_2 to differ from 180°, resulting in nonzero $|V_{RF,out}|$ even if $|A_1| = |A_2|$, as well as a more gradual phase shift as the null is crossed. A series inductor (L_s in the figure) resolves this issue by nullifying the effect of Z_L's capacitive component. Combined, the null created by A_2 tuning and minimized by inductive-capacitive resonance produces sensitive $V_{RF,out}$. This is the basis of the AQC impedance measurement technique. Following I/Q mixing and post processing, $V_{RF,out}$ is manifested as $V_{BB,out}$.

III. Circuit Implementation

Fig. 2(a) shows a transistor-level implementation of the AQC [10], [11], with a variable resistor R_{tune} included as the tuning mechanism and a large capacitor C_{ac} to isolate DC bias points. R_{tune} needs to be set as low as a few Ω for A_2 to equal A_1, which poses two problems for the preceding buffer (Fig. 2(b)): the buffer consumes high current to make $R_{out} \ll R_{tune}$, and the large C_{ac} is needed. To address the above issues, we propose a "source-follower DAC" (SF DAC) (Fig. 2(c-e)) that merges R_{tune} with the buffer. This is accomplished by exploiting the SF DAC's output resistance to serve as R_{tune}, which can be controlled by switching in different numbers of parallel SF unit cells (controlled by D_{in}). This reduces the buffer power by about 20×. Additionally, the SF DAC eliminates C_{ac} by creating the needed level shift.

The proposed tunable AQC with SF DAC, as shown in Fig. 2(e), is built from unit cells (Fig. 2(d)), each consisting of

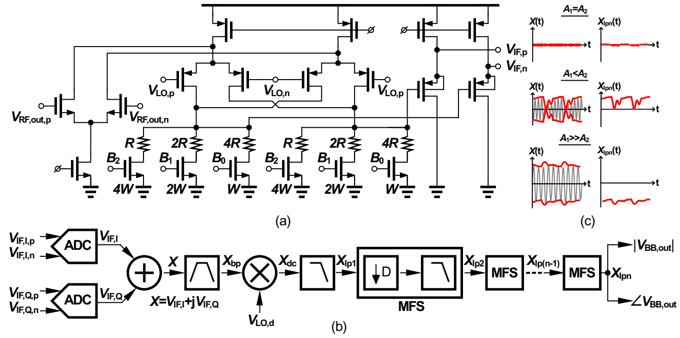

Fig. 3. (a) Double-balanced mixer with programmable gain to downconvert $V_{RF,out}$ to 1 MHz for digitization. (b) High-Q (>10,000) digital filtering using multirate processing to reduce signal to desired bandwidth. (c) Example output waveforms for three cases of relative values of A_1 and A_2.

an input transistor (M_A) with a current source (M_C) and an active load (M_L). From P1 to P3, the A_1 path acts as common-source and the A_2 path as common-gate, thus forming the $A_2 - A_1$ gain. From P1 to P2 and from P2 to P3, the same A_1 path also acts as common-drain and common-gate, respectively, thereby providing a low impedance at P2. The SF DAC is implemented as a combination of a binary-weighted number of parallel units configured as source followers, with each binary set switched at the load and current source gates. Z_L and R_{tune} affect the small-signal gain as follows (ignoring channel-length modulation and body effect to show the AQC nulling functionality in simple terms):

$$A_2 - A_1 = \frac{n_2 g_{m_2}(R_{D_5}/n_5)}{1 + n_2 g_{m_2} R_{tune}} - \frac{n_1 g_{m_1}(R_{D_4}/n_4)}{1 + n_1 g_{m_1} Z_L} \qquad (1)$$

where $R_{tune} = 1/(n_3 g_{m_3})$, n_i is the number of parallel unit transistors (for n_3, this is the number of units that are switched in), R_{D_i} is the unit load resistance, g_{m_i} is the unit transconductance, and i is the corresponding transistor number. The circuit produces a null when the tuning parameter n_3 is set so that $A_1 = A_2$.

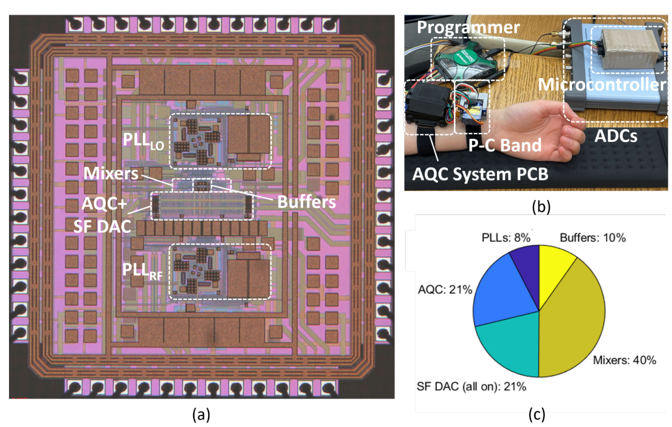

Fig. 4. (a) Die photograph. (b) Setup for human plethysmographic monitoring. (c) IC power consumption breakdown.

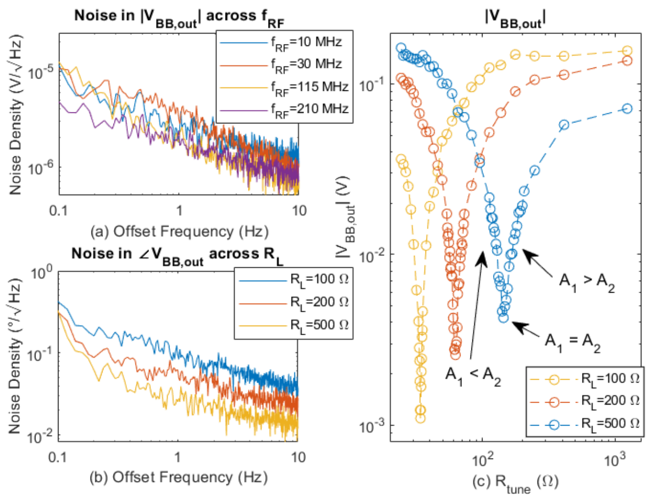

Fig. 5. (a) Measured noise density in $|V_{BB,out}|$ for $R_L = 100$ Ω. (b) Measured noise density in $\angle V_{BB,out}$ for $f_{RF} = 210$ MHz. (c) Measured $|V_{BB,out}|$ v. R_{tune} for three Z_L values at $f_{RF} = 10$ MHz.

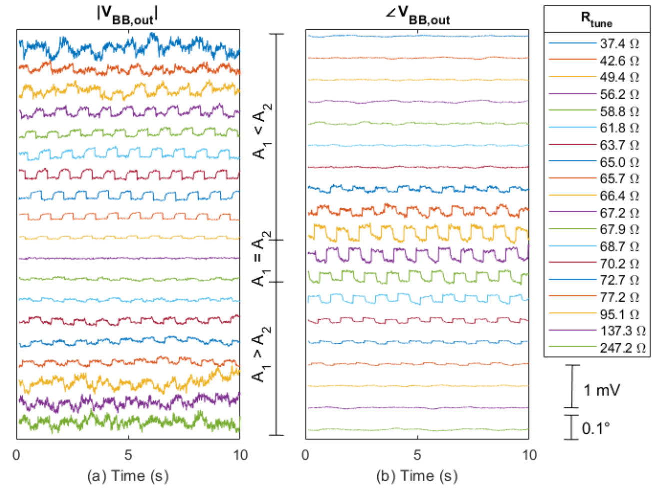

Fig. 6. Sensitivity demonstration showing measured 1-Hz square pulse in Z_L from 214.00 Ω to 214.37 Ω at $f_{RF} = 10$ MHz, $BW = 48$ Hz.

The AQC outputs are downconverted by double-balanced I/Q mixers (Fig. 3(a)). The loads are programmable with binary-weighted resistances R to adjust the mixer gain. The mixers feed into source follower buffers whose outputs exit the IC, where they are sampled and processed as depicted in Fig. 3(b). X is formed as $IF_I + jIF_Q$ and then bandpass-filtered and downconverted to DC using a digital $V_{LO,d}$. For high-Q (>10,000) filtering, X_{dc} is lowpass-filtered and then fed through a series of multirate filtering stages (MFS), which consist of downconversion by a factor of D followed by lowpass filtering with normalized corner frequency $1/(2D)$. Fig. 3(c) displays example waveforms showing the carrier (1 MHz) of signal X filtered out at X_{lpn}. The output signal X_{lpn} has far fewer samples ($(n-1)D$) and a bandwidth which is large enough to capture ~20 harmonics of the fundamental frequency of a human pulse (~1-2 Hz) and small enough to suppress out-of-band noise (e.g., 48 Hz). For comparison with other plethysmography systems, plethysmographic signals are further filtered to a bandwidth of 4 Hz, where the RMS noise for a 100-Ω load is only 1.5 mΩ_{rms} in both $|V_{BB,out}|$ and $\angle V_{BB,out}$ when $f_{RF} = 115$ MHz and 210 MHz, respectively.

IV. Measurement Results

Fabricated in a 180-nm CMOS process, the chip (Fig. 4(a)) occupies an active area of 0.325 mm^2. Fig. 4(b) shows the setup for human measurements, with the AQC system PCB controlled by a programmer, a pressure-controlled (P-C) band controlled by a microcontroller, and the system output sampled by external analog-to-digital converters (ADCs). Fig. 4(c) shows the power distribution, with the IC consuming 45.8 mW at the highest value of R_{tune} (32.2 mW at the lowest).

The IC is first tested with Z_L consisting of a resistor (R_L), with L_s excluded. Noise is measured for $R_L = 70$ Ω, 100 Ω, 200 Ω, 500 Ω, and 3.6 kΩ at $f_{RF} = 10$ MHz, 30 MHz, 115 MHz, 210 MHz, and 220 MHz. A subset of the measured input-referred noise density curves is plotted in Figs. 5(a) and 5(b). The noise performance is summarized in Table I. Fig. 5(c) shows $|V_{BB,out}|$ v. R_{tune} for various R_L values. As annotated on the $R_L = 500$ Ω curve, $|V_{BB,out}|$ exhibits the expected high derivative where $A_1 < A_2$ and where $A_1 > A_2$, and the expected null where $A_1 = A_2$.

Next, the IC's sensitivity is tested with Z_L consisting of a periodically time-varying resistor, with L_s excluded. Fig. 6 demonstrates the capability of the nulling function to enhance sensitivity to small changes in Z_L. The figure shows a 1-Hz pulse in Z_L between 214.00 Ω and 214.37 Ω at $f_{RF} = 10$ MHz. These Z_L values are chosen based on realistic expectations for baseline and plethysmographic variation of human tissue impedance. $|V_{BB,out}|$ and $\angle V_{BB,out}$ are plotted across many R_{tune} values, with the phase data detrended

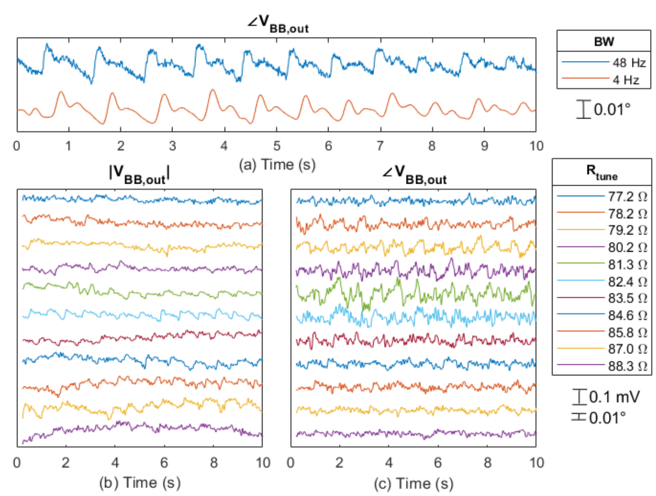

Fig. 7. (a) Human plethysmographic signal at $f_{RF} = 130$ MHz and $R_{tune} = 26.6$ Ω. (b) Human plethysmographic signals showing sensitivity variation across R_{tune} values at $f_{RF} = 112$ MHz, $BW = 24$ Hz.

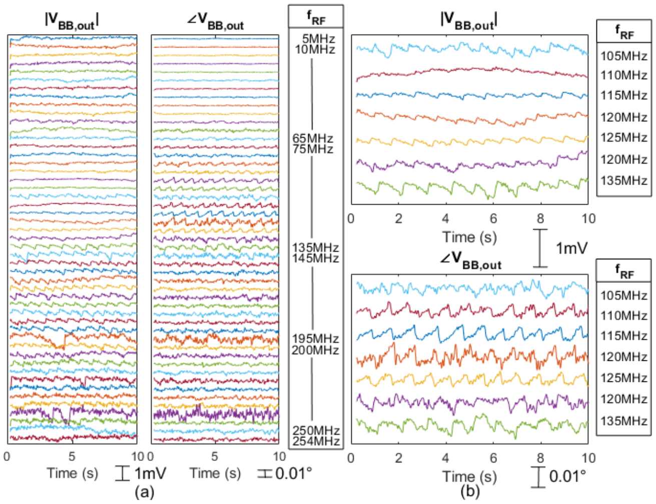

Fig. 8. (a) Human plethysmographic signals showing spectroscopic capability (from $f_{RF} = 5$ MHz to 254 MHz) at $R_{tune} = 26.9\ \Omega$. (b) Close-up of subset of signals in (a).

TABLE I
PERFORMANCE SUMMARY AND COMPARISON

	This Work	[12] JSSC '23	[13] JSSC '19	[14] JSSC '14	[15] TBioCAS '10
Application	Spectroscopic Plethysmography	Plethysmography		Spectroscopy	
Tech. (μm)	0.18	0.18	0.055	0.35	0.35
Freq. (Hz)	1M-255M	1k-215k	1k-1.024M	1k-150M	10-50M
Demonstrated Pleth. Freq.	5M-254M	<215k	32k, 128k	N/A	N/A
Baseline Cancellation?	Yes	Yes	Yes	No	No
Excitation On-Chip?	Yes	No^i	No^j	No	No
Core Area (mm^2)	0.325	1.92	0.74	1.6^a	4^{a,b}
Supply (V)	1.8	1.8	1.2	3	3.3
Power (mW)	45.8^c	0.4725^c	0.1896^c	112.5	84.8^b
Input-Referred Noise Density (m$\Omega/\sqrt{Hz}$)	$\lvert V_{BB,out}\rvert$: 0.8^f $\angle V_{BB,out}$: 0.7^g (@1Hz; 100Ω)	0.5^k (@1Hz; 100Ω)	0.6 (@1Hz; 100Ω)	N/A	N/A
Input-Referred RMS Noise (mΩ_{rms})	$\lvert V_{BB,out}\rvert$: 1.5^f $\angle V_{BB,out}$: 1.5^g (0.1-4Hz; 100Ω)	1.0 (0.1-4Hz; 100Ω)	1.2 (0.1-4Hz; 100Ω)	N/A	N/A
Reported Performance Metric	Dynamic Range (dB):^{l} $\lvert V_{BB,out}\rvert$: 120.6^h $\angle V_{BB,out}$: 128.0^e (BW=4Hz) Max SNR (dB):^{m} $\lvert V_{BB,out}\rvert$: 88.0^d $\angle V_{BB,out}$: 97.6^f	Dynamic Range (dB): 145.2 (BW=4Hz), Max SNR (dB): 103.5	Dynamic Range (dB): 141 (BW=4Hz)	Capacitance Resolution: 0.6 aF @150MHz (BW=10Hz)	Current Sensitivity: 300 pA (BW=10Hz) (0.5-2.4GHz)

[a]Chip area; [b]Array; [c]Worst case; [d]@10MHz; [e]@30MHz; [f]@115MHz; [g]@210MHz; [h]@220MHz;
[i]Includes current generator but does not specify whether frequency generation is on-chip;
[j]Includes current generator but requires external frequency generation; [k]$Z_{rms}/\sqrt{BW}$;
[l]$20\log_{10}(Z_{L,max}/(2\sqrt{2} \times Z_{rms,min}))$, where $Z_{rms,min} = Z_n \times \sqrt{BW}$;
[m]$\max(20\log_{10}(Z_L/(2\sqrt{2}Z_{rms})))$, where $Z_{rms} = Z_n \times \sqrt{BW}$ and Z_n is noise density

to remove a low-frequency drift. The maximum sensitivity appears where expected: at $A_1 = A_2$ in $\angle V_{BB,out}$ (Fig. 6(b)) and near $A_1 = A_2$ in $|V_{BB,out}|$ (Fig. 6(a)), with near-zero sensitivity in $|V_{BB,out}|$ where $A_1 = A_2$.

Finally, the IC's ability to measure plethysmographic signals is tested on human subjects (approved under BYU IRB #F2020-268; consent obtained) using the setup of Fig. 4(b). The setup includes safety circuitry (for IEC 60601-1 compliance), an inductor (L_s) to resonate with the human tissue capacitance, two electrodes in contact with the human wrist directly over the radial artery, and a P-C band to minimize artifacts related to pressure variation. The electrodes are made of carbon, 8 mm long by 2 mm wide with 6 mm spacing center-to-center. Fig. 7(a) shows a $\angle V_{BB,out}$ signal measured on Subject 1 at different bandwidths (48 Hz, 4 Hz). Fig. 7(b) and 7(c) show $|V_{BB,out}|$ and $\angle V_{BB,out}$ across many R_{tune} values on Subject 2. The data produce the highest sensitivity in $|V_{BB,out}|$ at $R_{tune} = 82.4\ \Omega$ and in $\angle V_{BB,out}$ at 81.3 Ω.

Fig. 8 demonstrates spectroscopic capability on Subject 2, with Fig. 8(a) displaying signals across the IC's frequency spectrum with $R_{tune} = 26.9\ \Omega$. Due to the human tissue's complex nature, Z_L changes with frequency. Thus, the data show highest sensitivity around $f_{RF} = 105$–135 MHz (as displayed in Fig. 8(b)), where the system is near both resonance and the null. This real-time frequency shifting, combined with the tuning capability, demonstrates the proposed system's strengths for spectroscopic plethysmography monitoring.

Table I provides a performance summary and comparison with state-of-the-art. This work is first to measure spectroscopic plethysmography, and it does so in a frequency range not previously demonstrated by plethysmography systems. It also employs a novel baseline cancellation technique which uniquely creates sensitivity in both output magnitude and output phase. In addition, this work integrates the excitation signal generation on-chip, and the power figure is lowest among the systems in our frequency range. Thus, this system offers a powerful yet miniaturized platform for spectroscopic impedance plethysmography up to 255 MHz, enabling enhanced glucose–impedance correlation studies currently not possible with the existing solutions.

V. CONCLUSION

We present a spectroscopic impedance plethysmography IC to enhance future studies on blood glucose–impedance correlations. At the IC's core is an active quasi-circulator to maximize sensitivity and a novel source-follower DAC which buffers the excitation signal while providing tuning capability. On-chip excitation signal generation covers a frequency range of 1–255 MHz, and I/Q mixers downconvert the output for digitization. We demonstrate, for the first time, spectroscopic plethysmography for resonance-based measurements through electrical and human test results.

REFERENCES

[1] A. Caduff *et al.*, *Biosens. Bioelectron.*, vol. 19, no. 3, pp. 209–217, 2003.
[2] ——, *Biosens. Bioelectron.*, vol. 22, no. 5, pp. 598–604, 2006.
[3] S. Abasi *et al.*, *ACS Meas. Sci. Au*, vol. 2, no. 6, pp. 495–516, 2022.
[4] A. Kandwal *et al.*, *TIM*, vol. 72, pp. 1–15, 2023.
[5] A. V. Moço *et al.*, *Sci. Rep.*, vol. 8, no. 8501, 2018.
[6] T. Y. Abay and P. A. Kyriacou, *J. Clin. Monit. Comput.*, vol. 32, no. 3, pp. 447–455, 2018.
[7] Medis. Impedance-plethysmography (IPG).
[8] T. Deng *et al.*, *Ann. Palliat. Med.*, vol. 10, no. 3, 2021.
[9] V. Coulic *et al.*, *EMIJ*, vol. 6, no. 5, 2018.
[10] B. Tang *et al.*, *MWCL*, vol. 29, no. 6, pp. 409–411, 2019.
[11] B. Tang and L. Geng, *J. Semicond.*, vol. 41, no. 11, 2020.
[12] C. S. Park *et al.*, *JSSC*, vol. 58, no. 7, pp. 2040–2052, 2023.
[13] H. Ha *et al.*, *JSSC*, vol. 54, no. 11, pp. 2969–2979, 2019.
[14] D. Bianchi *et al.*, *JSSC*, vol. 49, no. 12, pp. 2748–2757, 2014.
[15] A. Manickam *et al.*, *TBioCAS*, vol. 4, no. 6, pp. 379–390, 2010.